A Dynamic WPT System With High Efficiency and High Power Factor for Electric Vehicles

Ali Zakerian, Sadegh Vaez-Zadeh, *Senior Member, IEEE*, and Amir Babaki

***Abstract*—Dynamic wireless power transfer (WPT) for charging electric vehicles (EVs) overcomes some of the problems associated with EVs battery size and weight as well as distance range limitation and long charging duration. High efficiency and fixed output voltage of WPT systems are of great importance for reducing operating cost and facilitating battery charging, respectively. On the other hand, utilizing the maximum power transfer capability of a WPT system leads to a capital cost saving of the system. In this article, the product of transferred power efficiency and input power factor (η·PF) is regarded as a criterion to make near full usage of the system power transfer capacity as well as reduce the capital and operating cost of the system. An optimal frequency-tracking method is proposed to maximize η·PF of the system taking into account possible abrupt changes in the coupling coefficient of the WPT system due to deviations of EV from alignment with the track along the road. In addition, the output voltage of the system is regulated simultaneously by an on-line adjustment of the primary inverter duty ratio. The optimal frequency-tracking method and voltage regulation are validated by extensive simulation and experimental results.**

***Index Terms*—Dynamic charging, efficiency, electric vehicles (EVs), power factor, tracking algorithm, wireless power transfer (WPT).**

I. Introduction

ON-LINE wireless charging of in-motion electric vehicles (EVs) is considered as an emerging option for future transportation systems [1], [2]. Therefore, maximizing wireless power transfer (WPT) efficiency has been investigated in both design stage [3]–[5] and operation [6]–[9]. In addition, high input power factor (PF) reduces the volt–ampere (VA) rating of the WPT system, including that of the power electronic switches for a certain transferred power [10] or increases the transferred power for a given rating of the power supply [11]. Generally, the system operation at the secondary resonant frequency leads to a maximum efficiency; whereas, the resonant frequency of the primary and secondary sides is often considered identical in the literature [3]. In this situation, applying the resonant frequency leads to unity PF operation, maximum power transfer efficiency, and reduced inverter switching losses [12]. However, in practice, the resonant frequency of the two sides may not be the same. Thus, a simultaneous unity power factor operation and efficiency maximization cannot occur for each operating frequency, anymore. The efficiency and PF improvement is investigated independently in the literature. Input apparent power of such systems is presented as a function of coupling coefficient K and input voltage for both mono and bipolar primaries without considering efficiency maximization [13]. A unity power factor is sought by proposing *LCL*-tuned secondary with extra switching mode controlled converters for reactive power compensation [14]. In addition, adding a wave-shaping controller in the secondary side is proposed to ensure a unity power factor [15]. Although the power loss of the secondary coil decreases in this method, the maximum load power reduces. Tracking methods for maximizing efficiency are also proposed in the literature, using a coupling coefficient estimator and an extra buck-boost converter in the secondary side [16]. However, the estimation procedure is complicated. Furthermore, the extra converter increases the construction cost and the total power converter losses. Frequency tracking is also proposed to maximize the system efficiency by tuning the inverter voltage to reduce the input power [17]. Moreover, variations in the inductance of WPT coils and the effect of the resonant frequencies detuning on the system efficiency are studied. However, the system power factor is not considered in this study.

The load voltage must be regulated where the WPT system charges the EV battery or feeds the EV motor drive, directly. Thus, output voltage regulation methods are discussed in the literature [18]. Adjusting the system operating frequency in order to regulate the output voltage decreases the efficiency [19], [20]. On the other hand, maintaining a constant output voltage by using a secondary converter means more hardware [18]. In addition, using an extra converter in the primary side for the sake of output voltage regulation suffers from the same drawback [20].

In this article, the optimum performance of the WPT systems with different resonant frequencies in two sides is analyzed. A novel performance criterion taking into account both the system efficiency and the system power factor is considered to provide energy saving and high power transfer. A new optimum frequency, which fulfills both objectives, is found and tracked online by a tracking algorithm. Simultaneously, an output voltage

Manuscript received May 15, 2019; revised August 19, 2019 and October 23, 2019; accepted November 18, 2019. Date of publication November 30, 2019; date of current version March 13, 2020. This work was supported by the Iran National Science Foundation (INSF) through the Chair of Contactless and Wireless Power Transfer. Recommended for publication by Associate Editor J. Acero. *(Corresponding author: Sadegh Vaez-Zadeh.)*

A. Zakerian and A. Babaki are with the School of Electrical and Computer Engineering, College of Engineering, University of Tehran, Tehran 1417466191, Iran (e-mail: zakerian@ut.ac.ir; amir.babaki87@ut.ac.ir).

S. Vaez-Zadeh is with the Advanced Motion Systems Research Laboratory and Center of Excellence on Applied Electromagnetic Systems, School of Electrical and Computer Engineering, College of Engineering, University of Tehran, Tehran 1417466191, Iran (e-mail: vaezs@ut.ac.ir).

This article has supplementary downloadable multimedia material available at http://ieeexplore.ieee.org provided by the authors.

Color versions of one or more of the figures in this article are available online at http://ieeexplore.ieee.org.

Digital Object Identifier 10.1109/TPEL.2019.2957294

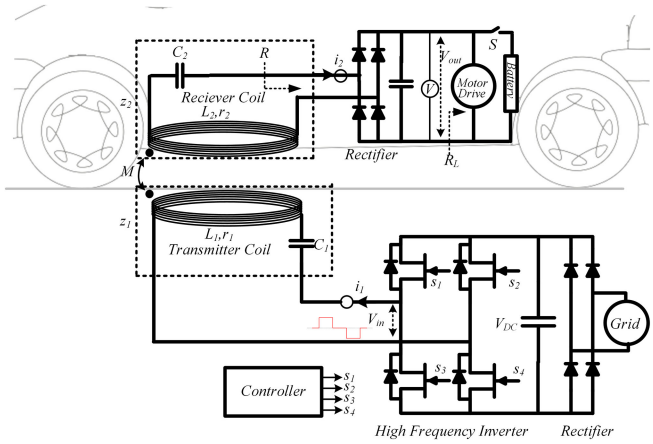

Fig. 1. WPT system model with series-series compensation.

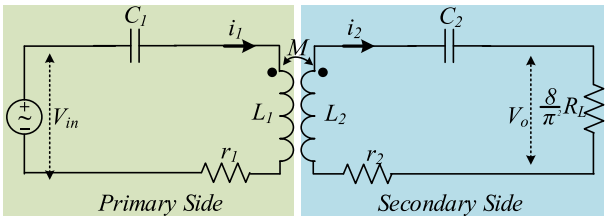

Fig. 2. Circuit model of the WPT system with series–series compensation.

regulation is sought by the online adjustment of the inverter duty cycle in the primary side against the variations of the coupling coefficient. Thus, no extra hardware is used for the optimum frequency tracking and voltage regulation in either side of the WPT system leading to a lower system cost and complexity. The simulation and experimental results of a WPT system under the proposed control system are presented to validate the control method.

II. System Modeling and Circuit Analysis

A typical WPT system with a series–series compensation circuit for EV charging is shown in Fig. 1. The system is modeled in the literature by an equivalent circuit as shown in Fig. 2. The primary and secondary windings are modeled with their coupled inductances L_1 and L_2 and resistances r_1 and r_2. The capacitors C_1 and C_2 are employed in series with the inductances in order to cancel the reactive power and increase the power transfer efficiency. The KVL equations of the circuit can be written as [21]

$$\bar{V}_{\text{in}} = z_1\bar{i}_1 - j\omega M\bar{i}_2 \tag{1}$$

$$z_2\bar{i}_2 - j\omega M\bar{i}_1 = 0 \tag{2}$$

where $\bar{i}_1$, $\bar{i}_2$, and $\bar{V}_{\text{in}}$ are the phasors of primary and secondary fundamental currents and fundamental inverter voltage, respectively. Impedances z_1 and z_2 belong to the primary and secondary side as they are shown in Fig. 1.

The efficiency of the WPT system is of great importance and is interpreted as a criterion for optimum operation of the system

TABLE I
Parameters of the System

Parameter		Value
L_1	*Primary side Inductance*	*129 μH*
L_2	*Secondary side Inductance*	*129 μH*
C_1	*Primary compensation capacitor*	*26.2 nF*
C_2	*Secondary compensation capacitor*	*26.2 nF*
r_1	*Resistance of primary coil*	*0.3 Ω*
r_2	*Resistance of secondary coil*	*0.1 Ω*
R_L	*Load resistance*	*9.25 Ω*
f_{r_p}	*Resonant frequency of primary side*	*86571 Hz*
f_{r_s}	*Resonant frequency of secondary side*	*86571 Hz*

[21]. It is obtained as [3]

$$\eta = \frac{P_{\text{out}}}{P_{\text{in}}} = \frac{P_{\text{out}}}{V_{\text{in}}i_1\text{PF}} = \frac{R}{(R_L + r_2)\left(1 + r_1\left(\frac{R+r_2}{(\omega_0 M)^2}\right)\right)} \tag{3}$$

where R is the equivalent resistance seen from the secondary rectifier. It can be converted to the load resistance, R_L, with a coefficient of $\pi^2/8$. Both R and R_L are shown in Fig. 1. On the other hand, the input PF of the system is a decisive factor in the effective utilization of the system power capability as explained in Section I. It is given as

$$\text{PF} = \frac{P_{\text{in}}}{S_{\text{in}}} = \cos\left(\tan^{-1}\left(\frac{\text{Im}(z_{\text{in}})}{\text{Re}(z_{\text{in}})}\right)\right) \tag{4}$$

where S_{in} and P_{in} denote the input apparent power (VA) and input active power of the WPT system, respectively. The input impedance of the system z_{in} can be written as [22]

$$|z_{\text{in}}| = \left|z_1 + (\omega_0^2 M^2/z_2)\right|. \tag{5}$$

Some investigations are carried out to find the optimum resonant frequency for WPT systems [3]. On the other hand, a resonanse frequency in the range of 81–90 kHz is selected for wireless EV charging systems according to SAE-J2954 standard [1]. The resonant frequency is determined here at 86571 Hz in conformity with the standard. A design procedure is then adopted to determine the system parameters in accordance with the selected resonant frequency [23]. The obtained parameters are presented in Table I.

III. Analysis of Efficiency and Power Factor

In this section, both system efficiency and power factor are considered in finding an optimum operating frequency. This is carried out by plotting η, *PF*, and η·PF versus the operating frequency in Fig. 3 according to (1) and (2) and their product with the parameters of Table I. In Fig. 3(a)–(c), the efficiency reaches its maximum value at a frequency of f_η, which is near the secondary resonant frequency. It is seen in Fig. 3(a) that if the resonant frequencies of primary f_{r_p} and secondary f_{r_s} are the same, the input power factor will be unity and the system efficiency is close to its maximum under an operating frequency equal to the resonant one [24]. However, in practice, there is no warranty that f_{r_p} and f_{r_s} are the same because the secondary side of the dynamic charging systems installed onboard is not the same for different EVs. So, the case of unequal f_{r_p} and f_{r_s}

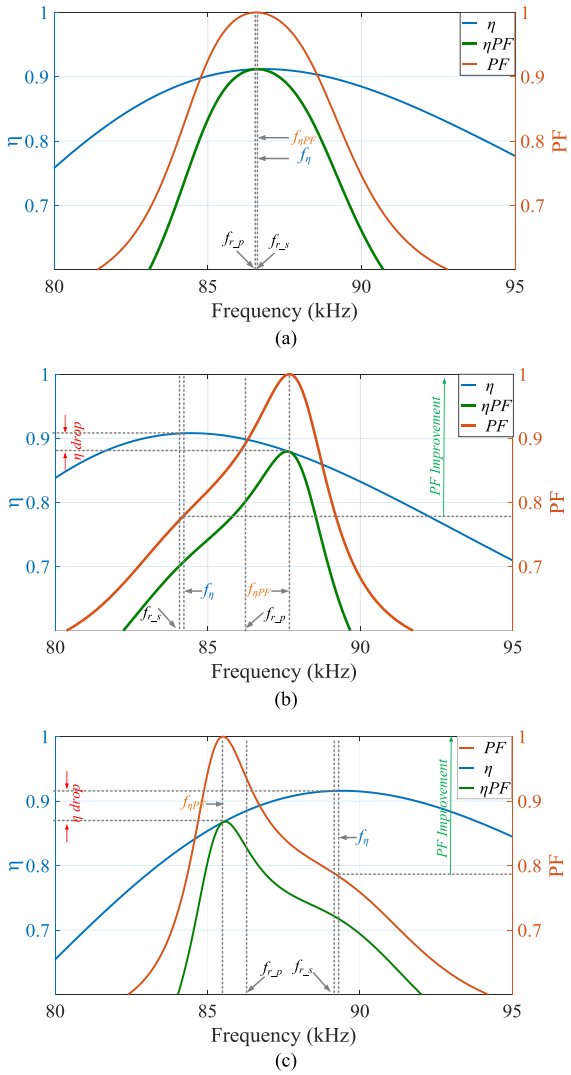

Fig. 3. Efficiency, power factor, and product of them versus frequency for $K = 0.075$: (a) equal f_{r_p} and f_{r_s}; (b) f_{r_s} less than f_{r_p}; and (c) f_{r_s} greater than f_{r_p}.

should be analyzed. For instance, if the compensation capacitor of the receiver on EV is 6% more than the transmitter's, then f_{r_p} and f_{r_s} would be 86 571 and 84 195 Hz, respectively. In this situation, η and PF are plotted versus the operating frequency in Fig. 3(b). Similarly, Fig. 3(c) shows these variables for a situation in which f_{r_s} is 2590 Hz more than its ideal value. So, in this case, f_{r_p} and f_{r_s} are 86 571 and 89 161 Hz, respectively.

It is seen that with unequal f_{r_s} and f_{r_s}, a high PF and a high efficiency will not be coincident at any system operating frequency. In fact, the system efficiency remains close to its maximum as far as the operating frequency is set at the secondary resonant frequency. However, at this frequency, the PF may deviate significantly from unity. Thus, the energy saving feature and the power capability utilization of the system are not fulfilled simultaneously.

Considering the above discussion, an optimal operating frequency other than the two side resonant frequencies may be found to provide a compromise between a high efficiency and a high PF. This will be possible by defining and maximizing an objective function incorporating both efficiency and PF. The contribution of η and PF in such an objective function would thus be a matter of investigation. Sophisticated multiobjective optimizations may be sought. However, a well established, effective, and straightforward criterion for many apparatuses and systems is the product of efficiency and power factor η·PF. This criterion has not been investigated for WPT systems in the literature so far. It is the intention of this article to focus on η·PF of WPT systems with unequal f_{r_s} and f_{r_s}. The criterion is obtained by multiplying (3) and (4) to yield

$$\eta \cdot \mathrm{PF} = \frac{1}{V_{\mathrm{in}}} \frac{P_{\mathrm{out}}}{i_1} = c \frac{P_{\mathrm{out}}}{i_1}. \tag{6}$$

It is interesting that (4), other than considering both PF and η, represents the output power per input current for a constant input voltage. Thus, maximizing η·PF at a constant V_{in} results in a minimum input current for a given load of the system. Nevertheless, if the inverter output voltage is adjusted by an output voltage regulation, V_{in} would not be constant during the system operation. Therefore, it is also possible to present η·PF as

$$\eta \cdot \mathrm{PF} = \frac{P_{\mathrm{out}}}{V_{\mathrm{in}} i_1} = \frac{P_{\mathrm{out}}}{S_{\mathrm{in}}}. \tag{7}$$

It is shown by (7) that η·PF can be regarded as a criterion to incorporate the power capability of the system through the input apparent power and rating of the primary power electronic switches, in addition to the performance of the WPT system through the output power of the system. Thus, maximizing (5) fulfills appropriate conditions for both power capability utilization and operating efficiency of the system. It is thus necessary to maximize η·PF of (7) by finding the optimum system operating frequency via calculating P_{out}, V_{in}, and i_{in} in terms of system impedances. It is plotted in Fig. 3(a)–(c) along with η and PF for a constant K. In case of $f_{r\_p} = f_{r\_s}$, the optimum frequency that maximizes η·PF, denoted by $f_{\eta\mathrm{PF}}$, is so close to f_η as it is seen in Fig. 3(a). In this case, operating the system under the common resonant frequency of two sides keeps both η and PF near their maximum values. However, in Fig. 3(b) and (c), in which $f_{r\_p} \neq f_{r\_s}$, $f_{\eta\mathrm{PF}}$ is not close to f_η. However, if $f_{\eta\mathrm{PF}}$ is selected as the operating frequency, PF will be improved substantially and reaches unity in both cases, whereas η drops a little bit from its maximum at f_η. Since the PF profile is more sensitive to the frequency variations than the efficiency profile, $f_{\eta\mathrm{PF}}$ is close to the frequency that maximizes PF.

By ignoring power losses in the secondary rectifier, the output power and current are readily given as

$$P_{\mathrm{out}} = V_{\mathrm{out}}^2 / R = V_{\mathrm{out}} \cdot i_2 \tag{8}$$

$$i_2 = V_{\mathrm{out}} / R. \tag{9}$$

Here, V_{out} is an RMS value of the fundamental voltage across the secondary rectifier. Hence, the input current is obtained as

$$i_1 = \frac{|z_2|}{\omega M} i_2 = \frac{|z_2|}{\omega M} \frac{V_{\mathrm{out}}}{R}. \tag{10}$$

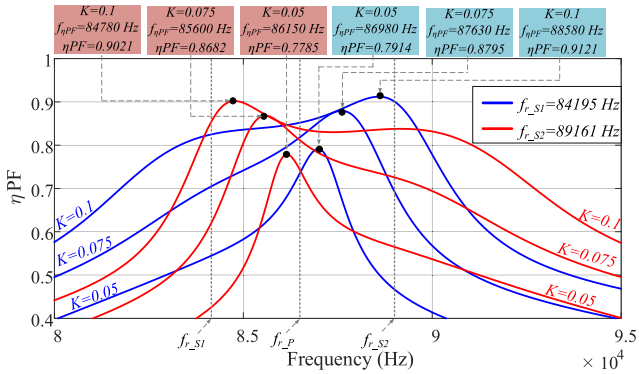

Fig. 4. Plot of η·PF versus frequency for two f_{r_s} of 84 195 and 89 161 Hz, while f_{r_p} is kept at 86 571 Hz.

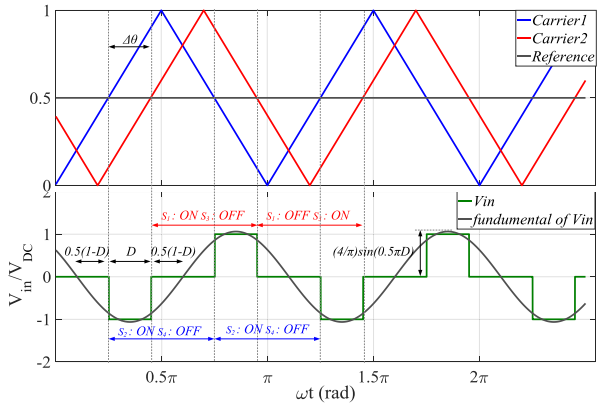

Fig. 5. Applied PWM method and the resultant output voltage.

In addition, the input voltage is given as

$$V_{\text{in}} = |z_{\text{in}}| \cdot i_1. \tag{11}$$

Using (8)–(11) in (7) yields

$$\eta \cdot \text{PF} = R\frac{\omega^2 M^2}{|z_1 z_2 + \omega^2 M^2|\,|z_2|}. \tag{12}$$

Substituting z_1 and z_2 into (12) in terms of the system parameters results in a complicated equation. Thus, a normalized angular frequency ω_n and a primary-side characteristic impedance λ, in addition to K, are defined for the sake of simplification as

$$\omega_n = \omega/\omega_{r\_p} = \omega\sqrt{L_1.C_1}$$

$$y = \omega_n^2 \tag{13}$$

$$\lambda = \sqrt{L_1/C_1} \tag{14}$$

$$K = M/\sqrt{L_1.L_2}$$

$$m = L_1/L_2. \tag{15}$$

Using (13)–(15) in (17), η·PF can be written as

$$\eta \cdot \text{PF} = \sqrt{\frac{R^2 m^2 K^4 y^5}{\lambda^2[A_1 y^6 + A_2 y^5 + A_3 y^4 + A_4 y^3 + A_5 x^2 + A_6 y + A_7]}} \tag{16}$$

where $A_1, A_2, \ldots$, and A_7 are functions of the system parameters. Equation (16) shows that η·PF varies with the changes in the operating frequency and K in a certain system.

The product of η·PF is maximized if f_{r_p} and f_{r_s} are equal. In the case of unequal resonant frequencies of the two sides, η·PF is shown in Fig. 4 for different coupling coefficients. While f_{r_p} is kept at 86 571 Hz, f_{r_s} is assumed to be 84 195 and 89 161 Hz, in order to analyze two cases of $f_{r\_p} > f_{r\_s}$ and $f_{r\_p} < f_{r\_s}$, respectively. It is seen that the maximum values of η·PF in Fig. 4 occurs in frequencies higher or lower than f_{r_p} for the lower and higher secondary frequencies, respectively.

The maximum value of (16), corresponding to the optimum frequency, cannot be obtained analytically due to its high degree. Therefore, an online tracking algorithm is proposed for reaching the optimum frequency.

As shown in Figs. 3 and 4, $f_{n\text{PF}}$ reaches f_{r_p} for loosely coupled systems. This is confirmed by Fig. 3, where the slope of PF is larger in value than the one of efficiency. Hence, PF dominates η·PF. Consequently, $f_{n\text{PF}}$ is close to the frequency that maximizes PF, i.e., f_{PF}. The maximum value of PF is unity regardless of the system parameters. Unity PF is realized if the input reactance x_{in} is zero. By using (13)–(15), x_{in} can be written as

$$x_{\text{in}} = \lambda\left[\left(\omega_n - \frac{1}{\omega_n}\right) - \frac{K^2\omega_n^2 m}{[(R+r_2)^2/\lambda^2] + (m\omega_n - 1/n\omega_n)^2}\left(m\omega_n - \frac{1}{n\omega_n}\right)\right]. \tag{17}$$

In WPT systems, $(R + r_2)^2 << \lambda^2$ and x_{in} can be estimated as

$$x_{\text{in}} \simeq \lambda\left[\left(\omega_n - \frac{1}{\omega_n}\right) - \frac{K^2\omega_n^2 m}{(m\omega_n - 1/n\omega_n)^2}\right] \tag{18}$$

where there is a K square in its second term. Thus, it decreases extremely at low values of K. Therefore, (18) can be estimated just by its first term. Hence, x_{in} approaches zero if ω_n gets close to unity. Therefore, $f_{\eta\text{PF}}$ gets close to the primary resonant frequency as $\omega_n = 1$ is equivalent to $f = f_{r\_p}$.

IV. Voltage Regulation

By using a full-bridge inverter, the three-level high-frequency voltage is built by using a PWM method based on the phase shift between carriers with a dc reference wave. As it is depicted in Fig. 5, the duty cycle and frequency of inverter output voltage are equal to the phase shift $\Delta\theta$ and the carrier wave frequency, respectively. Therefore, the optimum frequency can be adjusted by the frequency of carrier waveform. Moreover, V_{in} can be tuned by adjusting $\Delta\theta$.

The output load voltage must be kept constant to provide a constant voltage for the EV motor drive or battery. Using (1) and

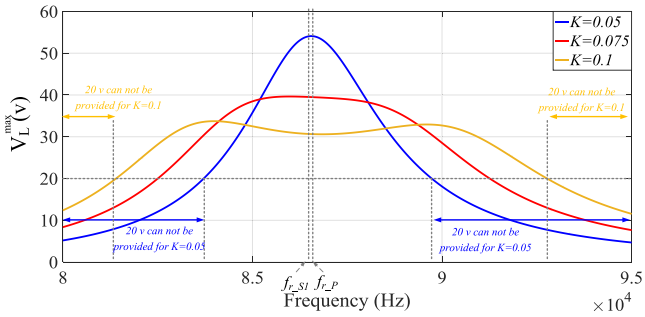

Fig. 6. Maximum possible load voltage versus operating frequency.

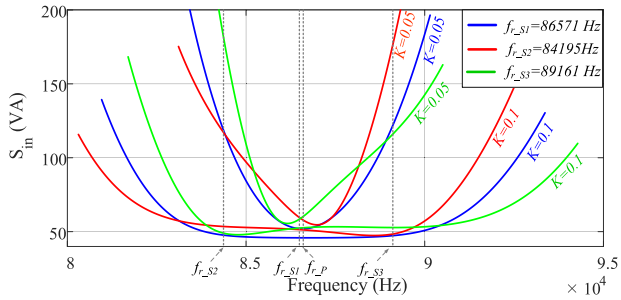

Fig. 7. Input apparent power versus operating frequency for equal and unequal primary and secondary resonant frequencies.

(2), the ac voltage delivered to the rectifier can be written as

$$V_O = i_2 R = \left(\frac{\omega M}{|z_2|} i_1\right) R = \frac{\omega M R}{|z_2|}\left(\frac{V_{\text{in}}}{z_{\text{in}}}\right) = \frac{V_{\text{in}} \omega M R}{|z_1 z_2 + \omega^2 M^2|}. \tag{19}$$

The fundamental harmonic of voltages, V_{in} and V_O, can be written as a function of V_{dc} and V_L, respectively, as

$$V_{\text{in}} = \frac{2\sqrt{2}}{\pi} V_{\text{dc}} \sin\left(\frac{\pi}{2} D\right) \tag{20}$$

$$V_O = \frac{2\sqrt{2}}{\pi} V_L \tag{21}$$

where V_{in} and V_O are depicted in Fig. 2. Using (19)–(21), V_L can be written as

$$V_L = \frac{R\omega M}{|z_1 z_2 + \omega^2 M^2|} V_{\text{dc}} \sin\left(\frac{\pi}{2} D\right) \tag{22}$$

where D is the inverter duty ratio and V_{dc} is the voltage of the primary dc link. It is seen that the load voltage is a function of the operating frequency and the mutual inductance, which may vary during the movement of EV. The maximum load voltage is obtained by assuming $D = 1$ in (22). This maximum possible load voltage $V_L^{\max}$ is shown versus the operating frequency in Fig. 6, while V_{dc} is 30 V. According to Fig. 6, the maximum possible load voltage has a peak value at the resonant frequency of system due to the cancellation of the imaginary parts of z_1 and z_2 in the denominator of (19). For loosely coupled systems, the peak value increases due to the stronger effect of M in the denominator of (19) compared with its nominator. It is seen that for loosely coupled WPT systems, the maximum possible voltage and inverter duty cycle are more sensitive to operating frequency due to the intense slope of maximum possible voltage around its maximum. Moreover, it is seen that the 20-V load voltage cannot be provided for some operating frequencies even with $D = 1$. Hence, for loosely coupled systems, a voltage regulation during tracking the optimum frequency is harder because the permitted searching frequency band is more limited.

From (12), (22), and Fig. 6, it can be declared that the optimum operation control and voltage regulation does not barricade each other if the operation frequency range is set sensibly. In other words, both control methods can achieve their goals, simultaneously.

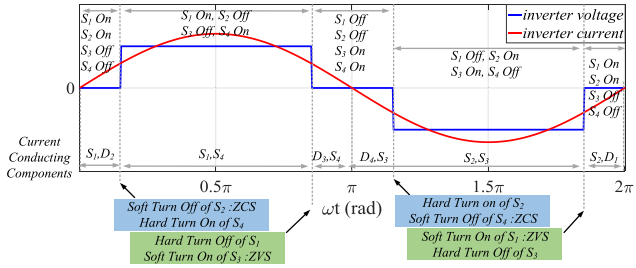

Fig. 8. Inverter soft switching with in-phase voltage and current.

The input apparent power is plotted in Fig. 7 with the determined duty cycle of the inverter. It is seen that for loosely coupled systems, the minimum required VA of the inverter has an intense slope along with the frequency band. Moreover, the minimum of S_{in} has a larger value for a lower K. Therefore, for a given output power, the minimum required VA of input power source is determined by the minimum coupling coefficient. The required input VA increases by more deviations from the resonant frequency of the system. If a frequency-tracking method is applied to the system, the required VA of the inverter is determined by the maximum and minimum possible operative frequency steps. Moreover, the discrepancy of the resonant frequencies increases the minimum required VA for a given load power.

Soft turn ON/OFF of power electronic switches is an important issue in resonant converters. By the applied PWM method, soft switching can be reached either with zero voltage switching (ZVS) or zero current switching (ZCS), regarding values of D and phase difference between the inverter output voltage and current φ. For instance, the inverter voltage and current are depicted in Fig. 8 while $\varphi = 0$.

As it is seen in Fig. 8, S_1 and S_3 are turned ON with ZVS. However, their turn OFF does not occur in zero current states. On the other hand, S_2 and S_4 have ZCS turned OFF and hard switching turned ON. Other conditions of D and φ can be analyzed similarly and are not elaborated here. However, a summary of the results are presented in Table II.

It is seen that soft switching may occur for all conditions except for $\varphi = 0$ and $D = 1$. In this specific situation, all the turning ON/OFF operations are hard switchings. In the other conditions, soft switching occurs either for turn ON or turn OFF. So by limiting the voltage regulation through $D<1$, the soft switching operation is assured.

TABLE II
SOFT/HARD SWITCHING OF INVERTER

	i_1		ZVS	ZCS
D=1	In phase		-	-
	Lag		S_1,S_2,S_3,S_4	-
	Lead		-	S_1,S_2,S_3,S_4
D<1	In Phase		S_1,S_3	S_2,S_4
	Lag	$\varphi>0.5(1-D)$	S_1,S_2,S_3,S_4	-
		$\varphi<0.5(1-D)$	S_1,S_3	S_2,S_4
	Lead	$\varphi>0.5(1-D)$	-	S_1,S_2,S_3,S_4
		$\varphi<0.5(1-D)$	S_1,S_3	S_2,S_4

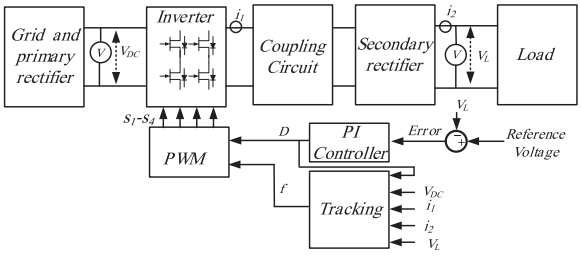

Fig. 9. Voltage regulation block diagram of the proposed system.

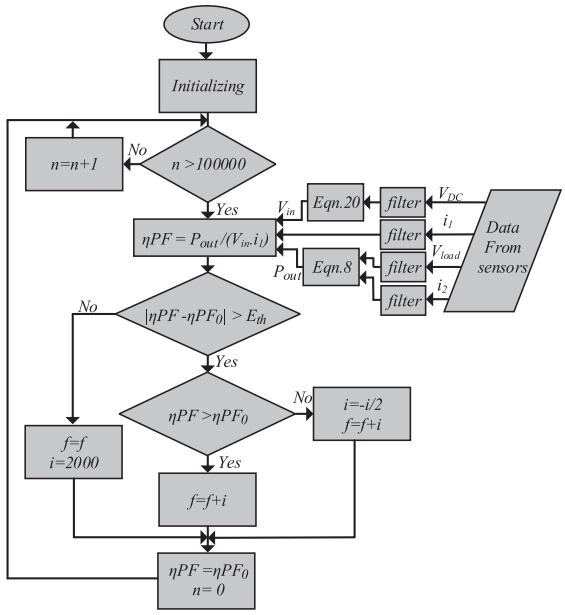

Fig. 10. Flowchart of the proposed control algorithm.

Comparing the proposed method with the method that uses the secondary resonant frequency as the system operating frequency, the switching loss decreases due to an almost unity power factor operation. This comparison is carried out for the case of unequal primary and secondary resonant frequencies. On the other hand, the resistance in the secondary winding and rectifier is the same for both cases due to the use of load voltage regulation. It must be mentioned that the conduction loss in the inverter switches and primary coil resistance increase due to the larger primary current in the proposed method.

V. CONTROL SYSTEM AND TRACKING ALGORITHM

The proposed control method has two goals including load voltage regulation and optimum frequency tracking. They are elaborated in this section.

A. Voltage Regulation

Several methods have been proposed for voltage regulation, usually by a particular converter [19]. The method proposed in this article needs no converter for voltage regulation as shown in Fig. 9. It is seen that the method uses samples of load voltage and compares them with the reference voltage to determine an error. A PI controller then adjusts D so that the output voltage is controlled at a constant value.

B. Optimum Frequency Tracking Algorithm

As it is explained in Section III, the global maximum of $\eta\cdot$PF is hard to be found analytically. Therefore, a tracking algorithm based on a numerical solution is proposed. The defined worst case determines the permitted frequency band over which the voltage regulation is possible. The minimum coupling coefficient for charging is set at 0.05 and the maximum deviation from the resonant frequency is supposed to be 3.5 kHz. Therefore, from Figs. 6 and 7 the operating frequency band is limited to 83–90 kHz. In this frequency band, the required VA of the power supply is 250 VA and a 20-V load voltage is reachable at all frequencies in the band.

Fig. 10 shows a flowchart of the tracking algorithm. The samples of inverter current and dc link voltage are required for tracking as well as the load voltage and current. It is notable that the high frequency sampling of $V_{\rm in}$ is difficult and is limited to low voltage values. In the proposed control method, $V_{\rm in}$ is calculated by (20). This calculation is simple enough because $V_{\rm dc}$ and D are provided by a dc link voltage sensor and the PI controller, respectively. In order to obviate the sampling distortion, the filters calculate the mean value of the last ten received data whenever a new data is received as

$$\text{mean}^{\text{new}} = 0.1(10\ \text{mean}^{\text{old}} + \text{data}^{\text{new}} - \text{mean}^{\text{old}}). \quad (23)$$

In the case of a misalignment of the primary and secondary windings, the obtained $\eta\cdot$PF decreases substantially. Therefore, the algorithm starts to find a new optimum frequency.

VI. PERFORMANCE EVALUATION

The proposed method is applied to a laboratory WPT system and its performance is validated by simulation and experimental results.

A. System Implementation

A WPT system with parameters of Table I is implemented as in Fig. 11. A design procedure as presented in the literature is used for determining the WPT system parameters [23]. The primary side is supplied by a voltage source H-bridge inverter that provides a 3-level high-frequency voltage. The WPT system resonant frequencies are 86 571 Hz for both the primary and secondary sides with the system parameters presented in Table I.

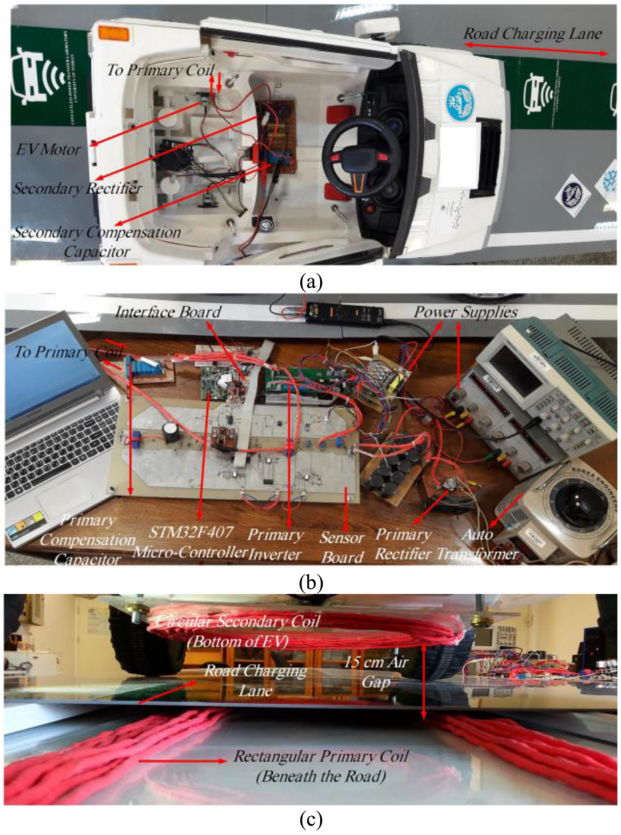

Fig. 11. WPT laboratory setup for online EV charging: (a) vehicle and its on-board system; (b) primary-side subsystem; and (c) primary and secondary coils.

For implementing cases that f_{r_p} and f_{r_s} are not the same, a resonant frequency of 84 195 Hz is set by 6% variation in the secondary compensation capacitor.

B. Simulations and Experimental Results

Using MATLAB Simulink and the WPT setup, comparative simulation and experimental results under the proposed control system are obtained as depicted in Figs. 12–14 under the variations of the coupling coefficient.

Fig. 12(a) and (b) compares the simulation and experimental results of online optimum frequency and maximum η·PF tracking before and after a coupling change, where f_{r_p} and f_{r_s} are 86 571 and 84 195 Hz, respectively. Comparing Fig. 12(a) and (b), it is evident that the results of simulation and experiment are in good agreement, which validates the proposed control system. According to Fig. 12(b), for $K = 0.1$, the system reaches a desirable steady-state performance by finding an optimum frequency at 88.75 kHz, in about 2 s in both simulations and experimental results.

A plot of η·PF for the WPT system, under the tracking algorithm is depicted in Fig. 13(a) and (b) by simulation and experimental results, respectively. It is seen that the system enjoys almost the same behavior by the simulation and experiment and reaches a maximum η·PF point at 0.91 and 0.89 at steady state by simulation and experiment, respectively. The small difference of

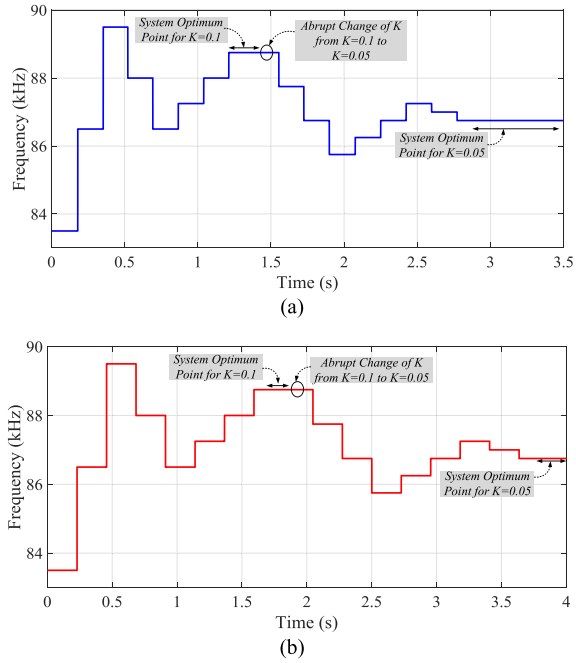

Fig. 12. Frequency variation under the optimum η·PF tracking: (a) simulation results and (b) experimental results.

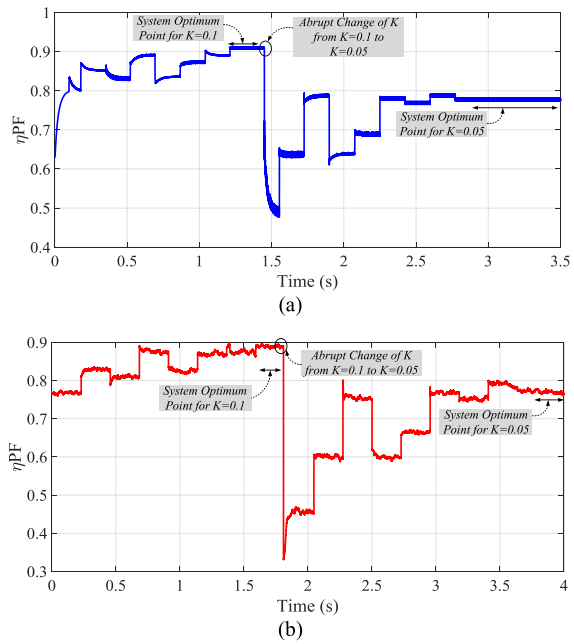

Fig. 13. Plot of η·PF during the tracking: (a) simulation results and (b) experimental results.

around 3%–5% between the simulation and measurement values of η·PF occurs due to ignoring the losses of the power converters in the simulation.

The changes of coupling coefficient cause a decrement of η·PF at $t = 1.48$ s and $t = 1.8$ s in the simulation and implementation, respectively. After a sudden drop of the coupling

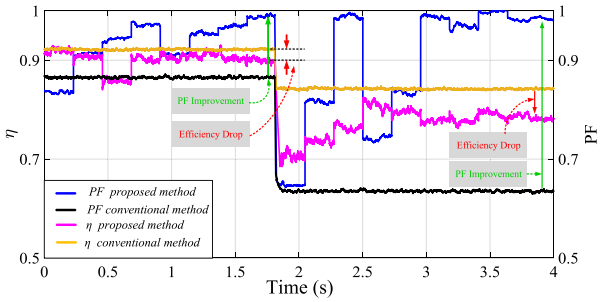

Fig. 14. Experimental results of η and PF in the conventional and proposed method.

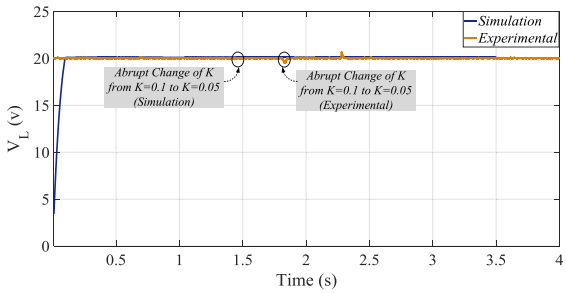

Fig. 15. Output voltage at the load terminal obtained by simulation and experiment.

coefficient from $K = 0.1$ to $K = 0.05$, the new optimum frequency is tracked. At $t = 2.75$ s and $t = 3.3$ s, the control system finds the new optimum frequency for new coupling coefficient by simulation and experiment, respectively. As a result, η·PF reaches its maximum values at 0.78 and 0.76 by simulation and experiment, respectively. They are lower than the previous maximum values of η·PF under the steady state. The experimental results of efficiency and power factor are depicted in Fig. 14 at the proposed optimum frequency and the conventional one which have been generally assumed to be equal to the secondary resonant frequency [16]. It is seen that by using the proposed method, the PF reaches unity approximately. Comparing with the conventional method, the PF increases substantially at the optimum operating points. On the other hand, the obtained efficiency in the proposed method is a bit lower than the one in the conventional method. Nevertheless, the drop in efficiency is much smaller than PF improvement.

The load voltage is regulated to its command value against the frequency with the ripples less than 5% as shown in Fig. 15 while the optimum frequency is being tracked. It is seen that the control system is robust against variations of the coupling coefficient since it keeps the output voltage constant at 20 V, while the coupling coefficient changes.

Simulation and experimental results are obtained for another case in which f_{r_p} is set to 2590 Hz less than f_{r_s}. The results are not presented here due to the limitation in space. Optimum frequencies of 85 and 86.25 kHz are obtained for coupling coefficients of $K = 0.1$ and $K = 0.05$, respectively.

In the optimum operation point of $K = 0.1$, the voltage and current waveforms of primary and secondary coils are shown

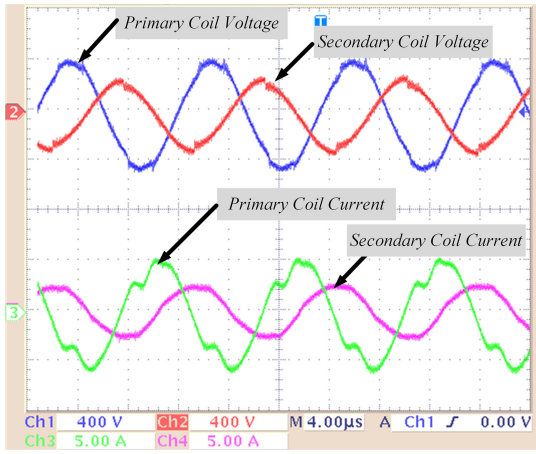

Fig. 16. Waveforms of primary coil voltage, secondary coil voltage, primary coil current, and secondary coil current.

in Fig. 16. The phase difference between voltage and current of each coil is influenced by the mutual inductance of the system. If the resonant frequencies of each side were equal and the operation frequency was set on the common resonant frequency, voltage and currents had about 90° phase shift for loosely coupled systems. However, this phase shift changes with an inequality of the resonant frequencies. The optimum frequency is close to the primary resonant frequency. This results in a near complete compensation in the primary side. Therefore, this phase difference is close to 90° for the primary side.

In order to evaluate the feasibility of the proposed method for in-motion EV charging applications, the dynamic of the system must be analyzed. A speed of 20 km/h for an EV on a charging lane 40-m long as the primary track is assumed [25]. A 7.2-s charging period is thus obtained. As it is observed in Fig. 15, the transient time for voltage regulation is less than 100 ms. As it is shown in Figs. 12 and 13, the tracking time for each coupling coefficient is less than 2 s, which is about 28% of the whole charging period. Therefore, the system operates efficiently in more than 72% of the charging time. It is notable that by applying the tracking process, the system reaches operating points that are close to the optimum point in a time period shorter than the whole tracking period. The remaining time is used to fine tune the operating frequency. Therefore, the system often operates near or at the optimum point.

VII. Conclusion

In this article, η.PF is introduced as a novel criterion to consider both efficiency and power capability transfer of WPT systems. It is shown that η.PF indicates output power per input VA. To optimize the system performance, a frequency-tracking method is proposed to ensure the optimum operation under varying coupling coefficient. In addition, the effect of inequality of primary and secondary resonant frequencies on η.PF is studied. In this situation, a maximum efficiency operation may not be provided for the WPT system by tracking the optimum frequency related to the maximum η.PF. However, it is shown that using the

optimum frequency, no significant drop in efficiency would happen. For keeping the load voltage constant, a voltage regulation method is used to adjust the switching duty cycle of the primary inverter. An experimental setup is implemented to validate the analytical and simulation results.

REFERENCES

[1] D. Patil, M. K. McDonough, J. M. Miller, B. Fahimi, and P. T. Balsara, "Wireless power transfer for vehicular applications: Overview and challenges," *IEEE Trans. Transp. Electrific.*, vol. 4, no. 1, pp. 3–37, Mar. 2018.

[2] S. Hasanzadeh and S. Vaez-Zadeh, "A review of contactless electrical power transfer: Applications, challenges and future trends," *Automatika*, vol. 56, pp. 367–378, 2015.

[3] S. Hasanzadeh, S. Vaez-Zadeh, and A. H. Isfahani, "Optimization of a contactless power transfer system for electric vehicles," *IEEE Trans. Veh. Technol.*, vol. 61, no. 8, pp. 3566–3573, Oct. 2012.

[4] R. Bosshard, J. W. Kolar, J. Mühlethaler, I. Stevanović, B. Wunsch, and F. Canales, "Modeling and η-α pareto optimization of inductive power transfer coils for electric vehicles," *IEEE J. Emerg. Sel. Topics Power Electron.*, vol. 3, no. 1, pp. 50–64, Mar. 2015.

[5] I. Karakitsios, F. Palaiogiannis, A. Markou, and N. D. Hatziargyriou, "Optimizing the energy transfer, with a high system efficiency in dynamic inductive charging of EVs," *IEEE Trans. Veh. Technol.*, vol. 67, no. 6, pp. 4728–4742, Jun. 2018.

[6] S. Li and C. C. Mi, "Wireless power transfer for electric vehicle applications," *IEEE J. Emerg. Sel. Topics Power Electron.*, vol. 3, no. 1, pp. 4–17, Mar. 2015.

[7] X. Tang, J. Zeng, K. P. Pun, S. Mai, C. Zhang, and Z. Wang, "Low-cost maximum efficiency tracking method for wireless power transfer systems," *IEEE Trans. Power Electron.*, vol. 33, no. 6, pp. 5317–5329, Jun. 2018.

[8] Z. N. Low, R. A. Chinga, R. Tseng, and J. Lin, "Design and test of a high-power high-efficiency loosely coupled planar wireless power transfer system," *IEEE Trans. Ind. Electron.*, vol. 56, no. 5, pp. 1801–1812, May 2009.

[9] A. Babaki, S. Vaez-Zadeh, and A. Zakerian, "Performance optimization of dynamic wireless EV charger under varying driving conditions without resonant information," *IEEE Trans. Veh. Technol.*, vol. 68, no. 11, pp. 10429–10438, Nov. 2019.

[10] D. Ahn and S. Hong, "A study on magnetic field repeater in wireless power transfer," *IEEE Trans. Ind. Electron.*, vol. 60, no. 1, pp. 360–371, Jan. 2013.

[11] W. Zhang and C. C. Mi, "Compensation topologies of high-power wireless power transfer systems," *IEEE Trans. Veh. Technol.*, vol. 65, no. 6, pp. 4768–4778, Jun. 2016.

[12] B. X. Nguyen *et al.*, "An efficiency optimization scheme for bidirectional inductive power transfer systems," *IEEE Trans. Power Electron.*, vol. 30, no. 11, pp. 6310–6319, Nov. 2015.

[13] F. Y. Lin, G. A. Covic, and J. T. Boys, "Differentiating coupling factor and VA transfer of IPT systems using bipolar pad primaries," in *Proc. IEEE Annu. Southern Power Electron. Conf.*, 2016, pp. 1–5.

[14] N. A. Keeling, G. A. Covic, and J. T. Boys, "A unity-power-factor IPT pickup for high-power applications," *IEEE Trans. Ind. Electron.*, vol. 57, no. 2, pp. 744–751, Feb. 2010.

[15] J. Boys, C.-Y. Huang, and G. Covic, "Single-phase unity power-factor inductive power transfer system," in *Proc. IEEE Power Electron. Spec. Conf.*, 2008, pp. 3701–3706.

[16] X. Dai, X. Li, Y. Li, and A. P. Hu, "Maximum efficiency tracking for wireless power transfer systems with dynamic coupling coefficient estimation," *IEEE Trans. Power Electron.*, vol. 33, no. 6, pp. 5005–5015, Jun. 2018.

[17] W. Fu, B. Zhang, and D. Qiu, "Study on frequency-tracking wireless power transfer system by resonant coupling," in *Proc. IEEE 6th Int. Power Electron. Motion Control Conf.*, 2009, pp. 2658–2663.

[18] H. Li, J. Li, K. Wang, W. Chen, and X. Yang, "A maximum efficiency point tracking control scheme for wireless power transfer systems using magnetic resonant coupling," *IEEE Trans. Power Electron.*, vol. 30, no. 7, pp. 3998–4008, Jul. 2015.

[19] N. Kim, K. Kim, J. Choi, and C.-W. Kim, "Adaptive frequency with power-level tracking system for efficient magnetic resonance wireless power transfer," *Electron. Lett.*, vol. 48, pp. 452–454, 2012.

[20] C.-S. Wang, O. H. Stielau, and G. A. Covic, "Design considerations for a contactless electric vehicle battery charger," *IEEE Trans. Ind. Electron.*, vol. 52, no. 5, pp. 1308–1314, Oct. 2005.

[21] D. H. Tran, V. B. Vu, and W. Choi, "Design of a high-efficiency wireless power transfer system with intermediate coils for the on-board chargers of electric vehicles," *IEEE Trans. Power Electron.*, vol. 33, no. 1, pp. 175–187, Jan. 2018.

[22] A. Zakerian, S. Vaez-Zadeh, A. Babaki, and M. F. Moghaddam, "Efficiency optimization of a dynamic wireless EV charging system using coupling coefficient estimation," in *Proc. 10th Int. Power Electron., Drive Syst. Technol. Conf.*, 2019, pp. 629–634.

[23] Y. Jiang, L. Wang, Y. Wang, J. Liu, M. Wu, and G. Ning, "Analysis, design, and implementation of WPT system for EV's battery charging based on optimal operation frequency range," *IEEE Trans. Power Electron.*, vol. 34, no. 7, pp. 6890–6905, Jul. 2019.

[24] J. M. Miller, O. C. Onar, and M. Chinthavali, "Primary-side power flow control of wireless power transfer for electric vehicle charging," *IEEE J. Emerg. Sel. Topics Power Electron.*, vol. 3, no. 1, pp. 147–162, Mar. 2015.

[25] J. Shin *et al.*, "Design and implementation of shaped magnetic-resonance-based wireless power transfer system for roadway-powered moving electric vehicles," *IEEE Trans. Ind. Electron.*, vol. 61, no. 3, pp. 1179–1192, Mar. 2014.